



Simulation performance of different planetary boundary layer schemes in WRF V4.3.1 on wind field over Sichuan Basin within “Gray zone” resolution

Qin Wang¹, Bo Zeng², Gong Chen², Yaoting Li¹

5 ¹Civil Aviation Flight University of China, Guanghan, China

²Institute of Plateau Meteorology, CMA, Chengdu/Heavy Rain and Drought-Flood Disasters in Plateau and Basin Key Laboratory of Sichuan Province, Chengdu, China

Correspondence to: Bo Zeng (bozeng126@126.com)

Abstract. The topography of Sichuan Basin is complex and unique, high-resolution
10 wind field simulation over this region is of great significance for meteorology, air
quality, and wind energy utilization. In this study, Weather Research and Forecasting
(WRF) model was used to investigate the performance of different planetary
boundary layer (PBL) parameterization schemes on simulating surface wind fields
over Sichuan Basin at a spatial resolution of 0.33km. The experiment is based on
15 multi-case studies, so 28 near-surface wind events from 2021 to 2022 were selected,
and a total of 112 sensitivity simulations were carried out by employing four
commonly used PBL schemes: YSU, MYJ, MYNN2, and QNSE, and compared to
observations. The results show that the wind direction which can be well reproduced,
is not very sensitive to the PBL schemes as the wind speed shows. As for wind speed,
20 the QNSE scheme had the best performance in reproducing the temporal variation out
of the four schemes, while the MYJ scheme had the smallest model bias. Further
cluster analysis demonstrates that the sensitivity of the PBL schemes is affected by
diurnal variation and different circulation genesis. For instance, when the surface
wind event caused by the southward movement of strong cold air and occurred during
25 6:00 and 8:00 (UTC), the variation and speed can be well reproduced by all four PBL
schemes and the differences between them are tiny. However, the simulation of
surface wind events mostly occurred during midnight and early morning, showing the
characteristics of poor RMSE and good COR, while the simulation results of the
evening-to-evening process and southerly wind process were opposite. Overall, the
30 four schemes are better for surface wind simulations in daytime than at night. The
results show the role of PBL schemes in wind field simulation under unstable weather
conditions, and provide a valuable reference for further research in the study area and
surrounding areas.

1 Introduction

35 Wind, as the most fundamental natural phenomenon in the atmosphere, poses not
only hazards to civil aviation safety and maritime transportation during severe wind
events (Manasseh and Middleton,1999; Leung et al.,2022), but also impacts the
dispersion of atmospheric pollutants directly near the surface, leading to adverse



40 effects on public health and the environment (Liu et al., 2020; Coccia, 2020; Yang and
Shao, 2021). What's more, wind energy has attracted increasing attention because of
its non-polluting and renewable nature, but due to the random nature of wind speed,
wind power generation is intermittent, which poses security and stability challenges
for large-scale integration of wind energy into the power network(Liu et al., 2019;
Kibona, 2020; Shi et al.,2021). Therefore, the accurate prediction of near-surface
45 wind farms has become the key to ensure traffic safety, optimize wind energy
utilization and evaluate air quality, and it is also an important scientific issue for
disaster prevention and mitigation, economic benefits and human life and health.

Near-surface wind fields are influenced by a combination of various factors,
including atmospheric thermal and dynamic conditions, topography, and underlying
50 surface (Zhang et al., 2021). As a state-of-the-art mesoscale weather prediction model,
the Weather Research Forecast (WRF) model can predict the fine-scale structure of
near-surface wind fields by simulating the evolution of various physical processes in
the atmosphere, which is significantly better than the prediction model based on
statistics which lacking the description of thermodynamic processes. Furthermore,
55 there are so many researches on the prediction and simulation of the refined
characteristics of local wind field by using WRF model (Prieto-Herráez et al., 2020;
Salfate et al., 2020; Xu et al., 2020; Tiesi et al., 2021; Wu et al., 2022; Yan et al., 2022;
Mi et al., 2023). Although the simulation of near-surface wind fields involves the
nonlinear interactions of various physical processes, the physical processes in the
60 planetary boundary layer (PBL) play a direct role in influencing near-surface wind
fields. As the interaction area between the atmosphere and the ground, the thermal
and dynamic structure, the turbulent motion and mixing process in the boundary layer
will directly affect the distribution of the near-surface wind field, so the simulation of
the boundary layer by the model can directly affect the accuracy of the near-surface
65 wind field(Chen et al., 2020).

In the mesoscale model, since the employed grid scales and time steps cannot
explicitly represent the spatiotemporal scales which turbulent eddies operate on, the
PBL parameterization scheme was used to express the effects of turbulent eddies
(Dudhia, 2014). The latest version of WRF model provides more than 10 kinds of
70 PBL parameterization schemes, the differences among them are mainly due to the
different methods of dealing with the turbulence closure problem, which further leads
to the different simulation result. Ma et al. (2014) conducted series sensitivity
simulations on spring strong wind events in Xinjiang by using the schemes of YSU,
MYJ, and ACM2, the results showed more downward transport of high-level
momentum in the YSU scheme. Studies by Wang et al. (2010) and Zhang and Yin
(2013) indicated that the ACM2 scheme performed well in simulating winter wind
conditions in Lanzhou city and Huangshan, Anhui. In addition, more studies have
shown that the MYJ scheme demonstrates the best simulation of near-surface wind
speeds in the coastal areas of Fujian (Yang et al., 2014), while in regions such as
75 western Neimenggu and Jiangsu, the YSU scheme exhibits the best forecasting
performance for 10-meters wind speeds (Cui et al., 2018; Li et al., 2018). In typical
mountainous terrain of Guizhou, the ACM2 scheme performs better in simulating
80



85 near-surface wind speeds at 70m height compared to the MYJ and YSU schemes (Mu et al., 2017). From these studies, it is evident that WRF has obvious regional performance regarding the PBL scheme. Therefore, without considering the nonlinear amplification of initial condition errors and the inaccuracy of numerical models, the reliable wind speed prediction for specific areas is still challenging and worthy of further study.

90 Sichuan Basin is one of the four major basins in China, it is bordered by the Qinghai-Tibet Plateau to the west, the Daba Mountains to the north, the Wushan Mountains to the east, and the Yunnan-guizhou Plateau to the south. Because of the complex terrain of its surrounding areas, the local atmospheric circulation is also complex and unique (Yu et al., 2020), the weather here is characterized by low wind speed, low sunshine and high humidity throughout the year, therefore it is also one of
95 the four major haze areas in China (Li et al., 2021). Under the unique terrain of the Sichuan Basin, it is difficult to determine whether cold air from mid to high latitudes can bypass the Qinghai-Tibet Plateau and then cross the Qinling Mountains to enter the basin. Besides, the basin effect makes it easier to form an inversion structure close to the surface and stabilizing the atmosphere (Gao et al., 2016; Feng et al., 2023).
100 These factors make it one of the regions with the poorest wind forecasting performance in China (Pan et al., 2021; Xiang et al., 2023). Therefore, wind is not still as wildly studied as temperature and precipitation in Sichuan Basin, and the main focus of wind simulation is about the pollutant diffusion under stable weather conditions.

105 As is known, the interaction between the surface and atmosphere, as well as the characteristics of turbulent motion over the basin terrain, differ from that over plains and plateau areas. However, there is no detailed evaluation for the performance of PBL schemes in the near-surface wind field over the Sichuan Basin. Thus, the present study aims at evaluating the performance of four PBL schemes under the windy
110 conditions over the Sichuan Basin. In the model set-up, a horizontal resolution of 0.3km was used for research, which is a major challenge in such region, because the spatial resolution is in the range of 0.1-1km, which is often referred as "gray zone" in numerical forecasting (Liu et al., 2018; Yu et al., 2022). As suggested by many studies, the spatial resolution in "gray zone", is too finely detailed with regarding to the mesoscale turbulence parameterization scheme, and too coarse for the Large Eddy
115 Simulation (LES) scheme to analyze turbulent vortices (Shin and Hong, 2015; Honnert et al., 2016). So far, the impact of different PBL schemes under the spatial resolution of "gray zone" is still uncertain. Hence, a total of 28 wind events is simulated with a purpose of getting a reliable evaluation, and the study is based on a
120 case study approach, rather than on continuous simulations. In general, this study not only has important significance for improving the wind field forecast in this region, but also provides a scientific basis for the further improvement and development of PBL scheme.

2 Data and Method



125 2.1 Data and experimental design

In this study, the experimental approach is different from what has been used in other studies, where one case or long continuous time is simulated. In this study, a total of 28 historical surface wind events was simulated by running WRF-ARW (version 4.3.1). We choose Guanghan Airport as the representative of Sichuan Basin, and the 28 discontinuous windy days, with a criteria of the maximum wind speed greater than 6 m s^{-1} are simulated.

The simulation domain consists of four two-way nested domains of resolutions 9 km, 3 km, 1 km and 0.33 km, with 105×105 , 103×103 , 103×103 and 103×103 grids, respectively, and the vertical resolution is 45 for all domains. Figure 1 presents the domain set-up. As can be seen from Fig. 1 (a), the outermost domain (D01) covers the western Sichuan Plateau and the northern Qinlin Mountains. The surrounding mountains are mostly between 1,000 and 3,000 meters above sea level, while the basin is between 250 and 750 meters. Due to the complex topography in the upstream region, the influence of cold air on the Sichuan Basin is variable, and the wind simulation is very difficult. In the western domain 2, the elevation gradually decreases from 2000 to 500 meters, with a topography that is higher in the western and northern parts, and lower in the eastern and southern parts. In the domain 4, the transitional zone from plateau to basin is avoided. This area is located in the northern part of Chengdu Plain, and the simulation center is set at Guanghan Airport (104.32° E , 30.93° N). Additionally, Guanghan Airport is located at the western foothills of the Longquan Mountains, only 10km away.

Given the complex terrain in study region and the high resolution of model design, the input of land surface data is particularly important, and its accuracy will directly affect the simulation of land surface processes and atmospheric boundary layer characteristics (Qi et al., 2021). Therefore, we replaced the terrain data of the 4-layer nested area with the 90 m resolution terrain data from the southwest region of Shuttle Radar Topography Mission (SRTM3).

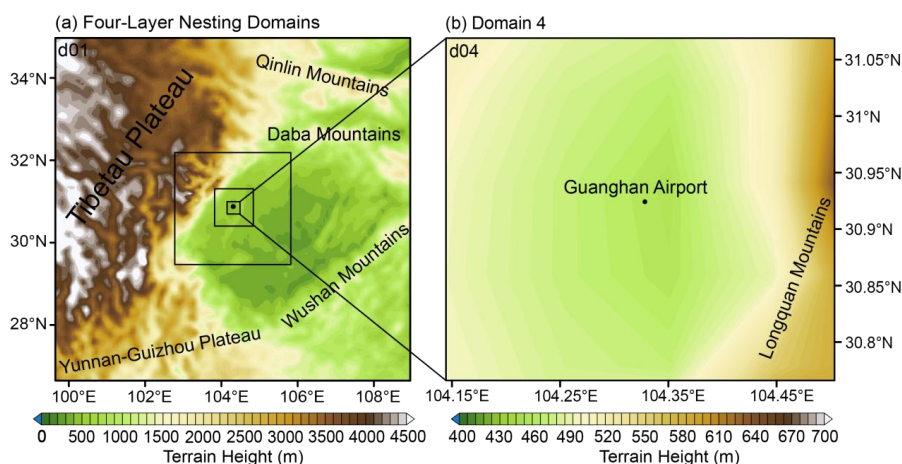


Figure 1. Configurations of (a) four-layer nesting domains (D01-D04) in WRF and the (b) study area. The spatial resolutions are 9, 3, 1 and 0.3 km, for domains D1 to D4, respectively. The figure depicts the actual orography implemented in the experiments.

To evaluate the model's ability in different PBL schemes, the observed wind fields at 10 meters high at Guanghan Airport station is used, The hourly reanalysis dataset ERA5 with a horizontal resolution of 0.25° and 38 vertical levels, is used to provide the initial and boundary conditions for WRF simulations, which are updated every 3 hours when input into the model. Each event is simulated using four different PBL parametrisation schemes. Thus, a total of 112 simulations are carried out. Each simulation spans 24 hours, with the corresponding high winds in the middle of the simulation, and discarding a spin-up period of 3 hours, the other model configuration is summarised in Table 1.

Table 1. Configures of the physical scheme in WRF simulation.

Parameterizations	Configuration
Micro-physical scheme	WSM 3-class graupel scheme (same for each domain)
Longwave radiative scheme	RRTM shortwave (same for each domain)
Shortwave radiative scheme	Dudhia shortwave (same for each domain)
Cumulus convection scheme	Kain-Fritsch for the outermost domain, and closed in other 3-layers

2.2 PBL Schemes

There are more than 10 PBL parameterization schemes in WRF-V4.3.1, but four commonly used PBL schemes were selected for this study, which are YSU (Yonsei



University) scheme (Hong et. al., 2006), MYJ (Mellor-Yamada-Janjic) scheme (Janjić,
 175 1990), MYNN2 (Mellor-Yamada- Nakanishi-Niino Level 2) scheme (Nakanishi and
 Niino , 2009) and QNSE (Quasi-Normal Scale Elimination) scheme (Sukoriansky and
 Galperin, 2006). Among them, YSU is a non-local, first-order closure scheme that
 represents entrainment at the top of the PBL explicitly, while the rest are local closure
 scheme, detail characteristics can be seen in Table 2. The surface layer scheme in the
 180 experiment is matched with each PBL scheme.

Table 2. Advantages description for the four PBL schemes used in WRF model.

Scheme	Advantages
YSU	1st-order closure scheme that is widely utilized for its robust representation of turbulence closure processes (Hong et. al., 2006).
MYJ	A 1.5-order closure scheme that is known for its effectiveness in capturing vertical mixing processes (Janjić, 1990).
QNSE	A 1.5-order closure scheme that improves the simulation of sub-grid scale turbulence (Nakanishi and Niino , 2009).
MYNN2	A 1.5-order turbulence closure scheme that accounts for both turbulent and non-turbulent mixing processes in the atmosphere (Sukoriansky and Galperin, 2006).

2.3 Statistical metrics for validation

185 As suggested by Wang et al. (2017), different sky conditions and atmospheric
 stability will affect the simulation of wind fields. So, in order to accurately evaluate
 the sensitivity of four PBL schemes to the near surface wind field in the western
 Sichuan Basin on the east side of the Qinghai Tibet Plateau, 28 surface wind cases
 with an 10 minutes averaged wind speed greater than 6 m s⁻¹ from 2021 to 2022 were
 190 selected for simulation, and the result is evaluated separately through different
 circulation patterns and K-means clustering analysis method. The main statistical
 metric used includes:

Root Mean Square Error (RMSE), which is the square root of the average of the
 squared differences between the simulated and observed values. RMSE is a
 195 commonly used metric in model evaluation, assigning higher weight to cases with
 larger simulation errors:

$$RMSE = \sqrt{\frac{\sum (O_i - S_i)^2}{N}} \quad (1)$$

where N is the total number of samples, O_i represents the observed surface wind,
 and S_i denotes the simulated surface wind, measured in m s⁻¹.

200 Correlation Coefficient (COR) is an indicator that measures the strength and
 direction of the linear relationship between simulation and observation. By analyzing



COR, the consistency between simulation results and observation results can be evaluated, and the corresponding PBL scheme can accurately capture the variation relationship of ground wind speed:

$$205 \quad \text{COR} = \frac{\sum_{i=1}^N (x_j - \bar{x}_j)(x_o - \bar{x}_o)}{\sqrt{\sum_{i=1}^N (x_j - \bar{x}_j)^2} \sqrt{\sum_{i=1}^N (x_o - \bar{x}_o)^2}} \quad (2)$$

where N is the total number of samples, x_o represents the observed values, and x_j denotes the simulated values.

210 Mean Error (ME) refers to the average difference between simulated and observed values, reflecting the overall bias of the simulation results. If ME is close to 0, it indicates that the simulation results have good accuracy at the average level. The calculation formula is as follows:

$$\text{ME} = \frac{1}{N} \sum_{i=1}^N (x_j - x_o) \quad (3)$$

215 The Weibull distribution is a probability function used to describe the distribution of wind speed. The expression for the Weibull distribution probability density function of wind speed v is:

$$f(v) = \frac{\kappa}{\lambda} \left(\frac{v}{\lambda}\right)^{\kappa-1} \exp\left[-\left(\frac{v}{\lambda}\right)^\kappa\right] \quad (4)$$

where k is the shape parameter, a dimensionless parameter, and λ is the scale factor, measured in m s^{-1} . These two parameters can be calculated using the following formulas:

$$220 \quad \kappa = \frac{\sigma}{\mu} \quad (5)$$

$$\lambda = \frac{\mu}{\left(0.568 + \frac{0.434}{\kappa}\right)^{\frac{1}{\kappa}}} \quad (6)$$

where σ and μ represent the standard deviation and mean value of the wind speed, respectively.

3. Overview of historical cases and evaluation of simulation results

225 3.1 Summary of 28 surface wind events

230 Since the experiment approach is concerned about multi-cases simulation in this study, it is necessary to understand the characteristics of these cases, such as the temporal variation, the peak time and dominated circulation, which can help to classify them and evaluate their simulation performance separately in the following analysis.

Therefore, Table 3 gives the detail information based on wind filed every 10 minutes. It is shown that out of the 28 surface wind events participating in the simulation, 24 were northerly events, accounting for 85% of the total. The events in



235 which the maximum wind is above 8 m s^{-1} accounts for 18%, and the events of $5\text{-}7 \text{ m s}^{-1}$ accounts for 82%. Meanwhile, the wind direction corresponding to the peak time was distributed between $350^\circ\text{-}50^\circ$, with northeasterly winds between $0\text{-}50^\circ$ being the most common. Additionally, the left are 4 southerly winds cases, all of which appear to occur in summer or early autumn. As for the dominated atmospheric circulation of each event, it is shown that most of the wind events were mainly caused
 240 by cold air, only little were associated with deep convection. Influenced by this, the spring (March-May) process accounted for the most, accounting for 46%, followed by summer and autumn, both accounting for 25%. In terms of the peak time, 60% of the simulated cases appear to concentrate on 05:00 - 09:00 UTC and 10:00 - 14:00 UTC at night, then followed by 15:00 - 19:00 UTC, and there are a total of 6 events
 245 occurred at 20:00 - 23:00 UTC and 00:00 - 04:00 UTC, accounting for 21%.

Besides, the observed wind rose and time series of wind speed are presented in Fig.2. It is indicated that during these periods, the near-surface wind is mostly from a northwesterly-to-northeasterly direction.

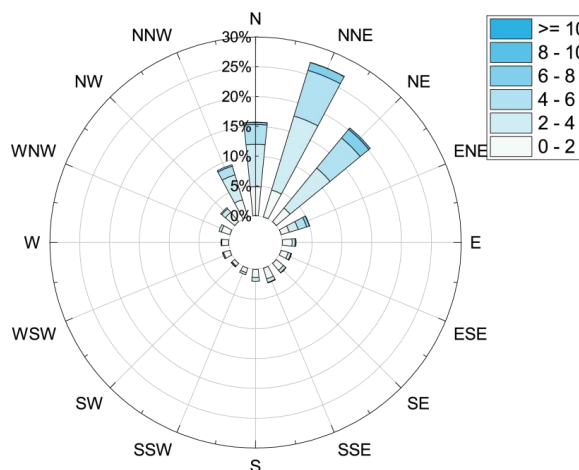
250 **Table 3.** Characteristics and circulation patterns of the 28 chosen near-surface wind events.

Event ID	Date yyyy-mm-dd	Maximum wind speed (m s^{-1}) /direction($^\circ$)	Maximum wind time hh:mm	Circulation classification
1	2021-03-17	6.0/350°	09:40	Cold air
2	2021-03-24	6.8/350°	08:00	Cold air
3	2021-03-30	6.1/90°	09:50	Cold air
4	2021-03-31	6.4/45°	09:00	Cold air
5	2021-04-23	6.3/47°	11:00	Cold air
6	2021-04-25	7.0/70°	08:00	Cold air
7	2021-04-27	8.3/18°	11:10	Cold air
8	2021-06-16	6.9/46°	07:40	Cold air
9	2021-07-21	7.1/158°	06:20	Deep convection
10	2021-08-22	8.0/47°	03:10	Cold air
11	2021-08-25	6.1/33°	06:00	Cold air
12	2021-09-15	6.6/50°	15:20	Cold air
13	2021-09-19	6.0/183°	08:00	Deep convection
14	2021-09-25	6.1/54°	05:00	Cold air
15	2021-10-01	6.0/332°	14:40	Cold air
16	2021-10-04	7.3/45°	03:30	Cold air
17	2021-11-06	9.6/51°	12:00	Cold air
18	2021-12-25	6.0/46°	20:50	Cold air
19	2022-03-19	7.9/10°	22:10	Cold air
20	2022-03-30	8.3/43°	12:20	Cold air
21	2022-04-14	6.0/27°	18:40	Cold air
22	2022-04-27	8.3/50°	17:00	Cold air

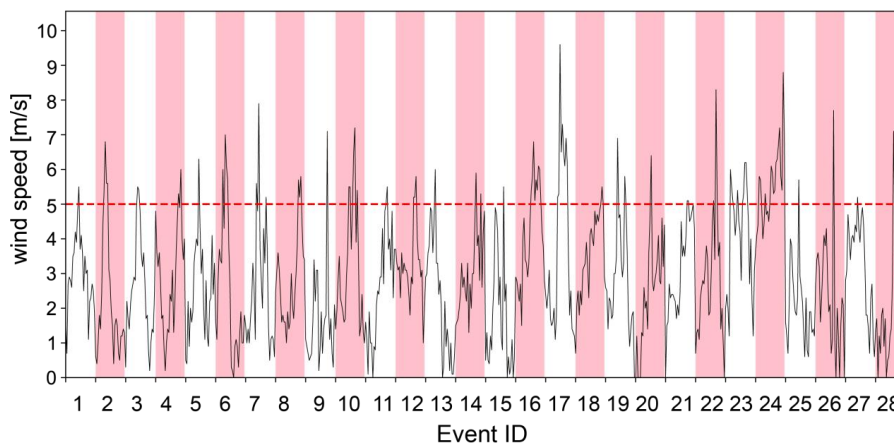


23	2022-05-08	7.1/26°	17:30	Cold air
24	2022-05-13	9.2/40°	22:40	Cold air
25	2022-06-23	6.2/119°	11:10	Deep convection
26	2022-08-17	8.6/148°	14:40	Deep convection
27	2022-08-28	6.7/40°	13:20	Cold air
28	2022-10-03	8.5/43°	02:40	Cold air

(a) Wind rose



(b) Time series of hourly 10-meters wind speed



255 **Figure 2.** Observed wind rose chart (a) and time series of hourly wind speed (b) for all the 28 near-surface wind events listed in Table 3. For the wind rose, the circles represent the relative frequency (%), and the colors represent wind speed.

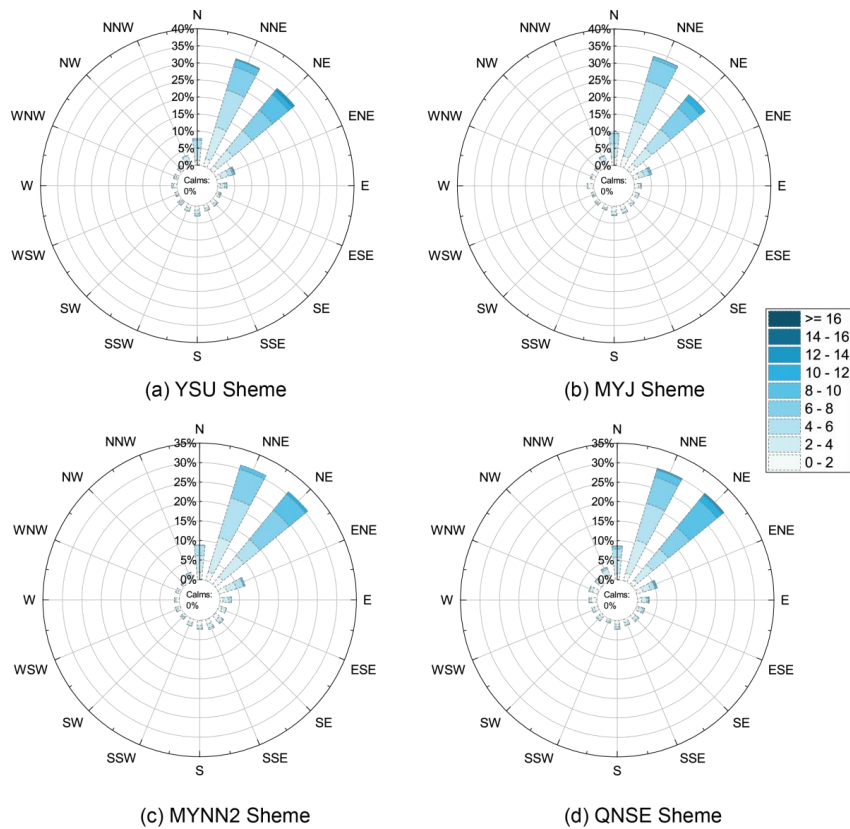
3.2 Overall simulation performance of 28 wind events

First, the performance of the model in different PBL schemes is assessed with



260 respect to wind direction. Thereby, the simulated wind rose of four PBL schemes are
given in Fig. 3. By comparing with the observation (Fig. 2), it is found that four PBL
schemes can reproduce the distribution of wind direction. Specifically, the simulated
wind directions are basically distributed in NNW, N, NNE, NE and ENE, reproducing
the characteristics of highly concentrating on NNE and NE. Besides, it is also shown
265 that all the PBL schemes tend to overestimate the prevailing wind direction and
significantly underestimate the NNW wind, indicating an clockwise bias which may
be related to the plateau topography with steep terrain in the northwest and west.
Therefore, it is concluded that the wind direction of the near-surface wind field in
Sichuan Basin is very insensitive to the selected PBL schemes.

270 However, there are still some differences in wind direction simulations among
four PBL schemes. In MYJ scheme, the frequency of NNE wind is higher than NE
wind, which is consistent with the observations. Moreover, the frequencies of N wind
and NE wind are closer to the observations. Therefore, MYJ has the best simulation
of wind direction. The wind direction distribution simulated by the MYNN2 scheme
275 is very close to QNSE scheme, but due to the worse performance in simulating NNW
wind and the larger frequency of simulated NNE and NE wind, MYNN2 scheme is
the worst among the four schemes. In general, for wind fields with weather processes
passing through, more attention is paid to the simulation of wind speed. So, we will
focus on the performance of wind speed next.



280

Figure 3. Same as in Fig. 2a, but for the simulated near-surface wind field corresponding to the four PBL schemes, the circles represent the relative frequency (%), and the colors represent wind speed

285 In fact, by comparing Fig. 2 and Fig. 3, it seems that all the four PBL schemes exhibit obvious exaggeration of wind speed, which is also shown in other numerous studies. But, what are the specific simulation characteristics of these commonly used PBL schemes in the Sichuan Basin? To further assess the advantages and disadvantages of each scheme in simulating surface wind speed, three statistics of COR, RMSE, and ME were selected for comprehensive evaluation of the simulation results, as shown in Fig. 4. In terms of COR, the mean and median correlation coefficients between simulation of the four schemes and observation are all between 0.4-0.6, and the median is above the mean value, indicating that the correlation coefficients are all negatively skewed distribution, that is, the correlation coefficients between simulated and observed wind speed are higher than the mean value in most cases, but very poor in some certain cases. It is further illustrated by the heat map displayed in Fig. 4d, where cases No. 3, 11 and 20 demonstrate correlation coefficients below 0. In contrast, QNSE shows the best mean correlation coefficient of 0.6, suggesting the best performance in reproducing the temporal variation of observed wind speed in most cases.

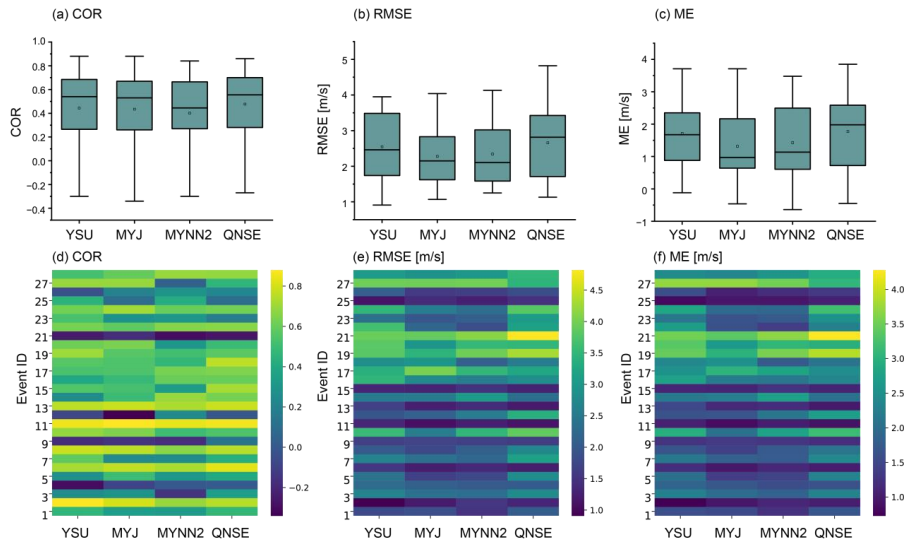
290

295



300 Although there is little difference between the simulated and the observed wind
speed in the RMSE and ME, it is interesting that MYJ scheme has the smallest RMSE
while QNSE has the largest. What's more, in MYJ scheme not only the ME is the
lowest (value is 0.96 m s^{-1}), but also the difference between the median and mean
values is significant, which suggests that most of the wind speed bias produced by
305 MYJ are actually below 0.96 m s^{-1} . Therefore, it is demonstrated that the bias of
near-surface wind speed produced by MYJ scheme in Sichuan Basin is the smallest
based on the multiple cases simulation. The main reason for this may be associated
with the basin topography, because the boundary layer is in stable condition in most
time, the turbulence is mainly generated and maintained by wind shear, so that the
situation showing strong locality. Therefore, the simulation error obtained by MYJ
310 scheme is the smallest in this stable and weakly stable boundary layer, which is
consistent with the research results of Zhang et al. (2012). Besides, the result that
QNSE scheme has the best performance on capturing the temporal variation of wind
speed, maybe because that QNSE scheme improves simulation of sub-grid scale
turbulence, and considers more complex and detailed physical processes. Under stable
315 atmospheric stratification, QNSE adopted $k-\varepsilon$ model developed from turbulent
spectral closure model, while under the unstable situation, the method of MYJ scheme
is used, so QNSE scheme has more advantages in the simulation of wind speed
variation trend.

320



325 **Figure 4.** Different performance metrics for the comparison of observed and simulated near-surface wind speed for 28 events. Box plots shows the overall characteristics of COR, RMSE and ME, and heat-map gives details for certain case. The box represents the metrics range from first quartile to third quartile, and the line inside the box represents the median, while the empty square represents the mean.

3.3 Differences of wind velocity segments and diurnal variations simulated by



four PBL schemes

Figure 5 shows the histogram of the frequency distribution of the observed and simulated wind speed at 10 meters high of the airport and the corresponding Weibull distribution fitting curve. As can be seen from the figure, the observed mode of wind speed is leftward, which is mainly due to the fact that the high wind speed sections are very concentrated and have a low frequency during 28 wind events. The corresponding Weibull fitting κ of the observation is 1.79, and the κ value produced by QNSE is the closest to it, while the fitting κ values of the other three schemes are all larger. The corresponding Weibull fitting λ values of the four parametric schemes are all larger than the observation (3.29 m s⁻¹).

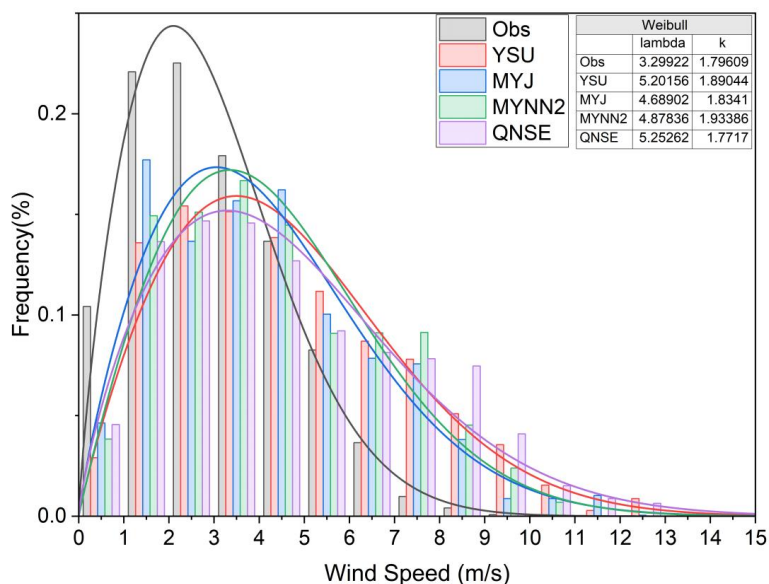


Figure 5. The frequency and Weibull fitting of the observed and four PBL schemes simulated wind speed of 28 wind events .

When wind speed below 3 m s⁻¹, none of the PBL scheme has a good performance. Moreover, the lower the wind speed, the greater the bias. In the range of wind speed greater than 3 m s⁻¹ and less than 5 m s⁻¹, different PBL schemes show significant differences compared with observations. Specifically for wind speeds during the 3-4 m s⁻¹, the simulation results of the MYJ scheme are closest to the observations, followed by MYNN2. For wind speeds during the 4-5 m s⁻¹, YSU and MYJ simulations are closer to the observations, indicating better performance in this wind speed range. All schemes tend to overestimate when wind speed above 5 m s⁻¹. Figure 6 further provides the deviations between the observed and simulated wind speed of four PBL schemes in different wind speed ranges. As can be seen, the performance of four PBL schemes differ greatly with the increase of wind speed, and



the wind speed deviation of the same PBL scheme also increases. For the wind speed
 below 3 m s^{-1} , the simulated wind of each PBL scheme are about $1.5\text{-}2 \text{ m s}^{-1}$ higher
 355 than the observation. In terms of mean values, the MYJ scheme exhibits relatively
 smaller deviations for wind speeds below 7 m s^{-1} , while the MYNN2 scheme
 demonstrates the smallest deviation in simulation for wind speeds above 7 m s^{-1} ,

In general, the fitting curve of QNSE scheme is most close to the observation,
 and the λ value is slightly to the right than the mode. The mode of four schemes are to
 360 the right relative compared with the observation, tending to a normal distribution.

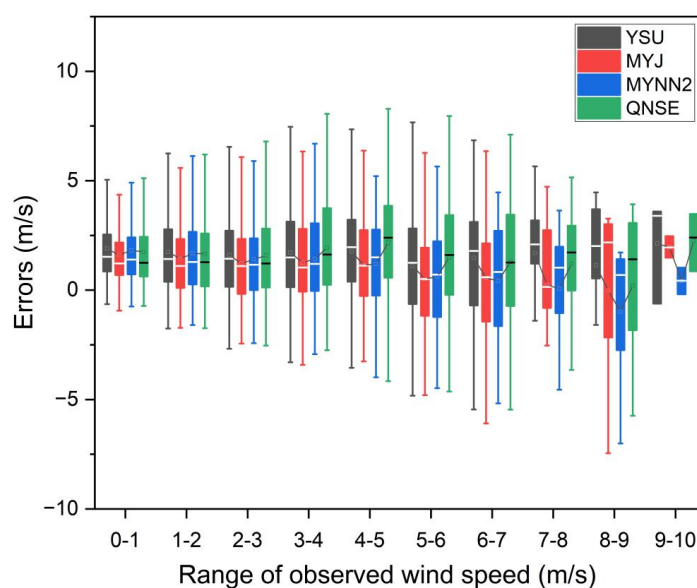


Figure 6. Wind speed errors of four PBL schemes in different wind speed segments for 28 wind events.

The variation of near-surface wind field is easily affected by surface
 365 characteristics, especially ground heating. When the weather background is fixed, the
 change of local thermal characteristics in a day will inevitably affect the near-surface
 wind field. Therefore, there will be significant differences in the wind field simulation
 during different time periods between different PBL schemes. According to the
 relationship between world time and local time, the daytime in the text corresponds to
 370 world time 00:00 - 10:00, and the nighttime refers to world time 11:00 - 23:00. Figure
 7 presents the diurnal variation characteristics of wind speed deviations simulated by
 the four PBL schemes in the WRF model through box plots.

In terms of the mean, the performance of wind speed of each scheme is better in
 the daytime than in the night. The deviation is the highest at 18:00 and 19:00 UTC,
 375 which means that the strong wind occurring at this time cannot be well simulated. As
 for YSU scheme, the simulation ability is the best at noon, while MYJ simulated well
 at noon and evening, and MYNN2 simulated in the evening. QNSE has little
 difference in the simulation of 28 wind cases in the daytime and a large difference in



the night, indicating that QNSE scheme is stable in the simulation of strong wind in
 380 the daytime, but unstable in the night, with a large variation of simulation
 performance. However, in general, QNSE scheme has the best simulation ability at
 noon.

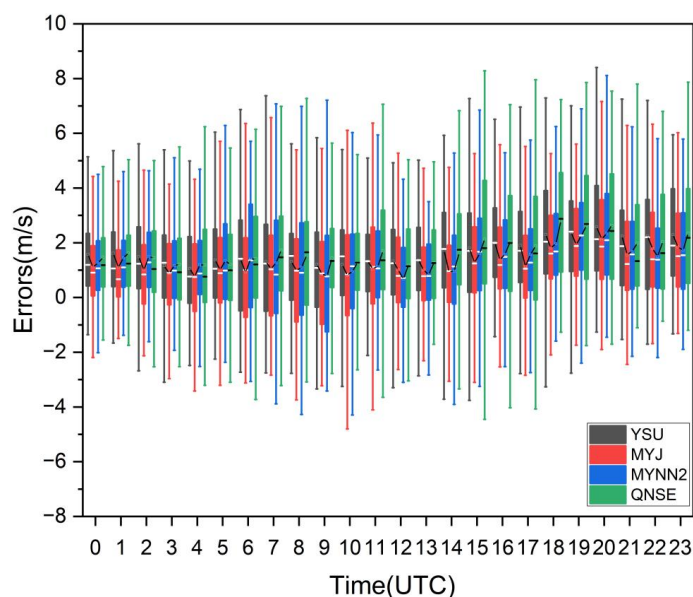


Figure 7. Diurnal variation of wind speed errors corresponding to four PBL schemes.

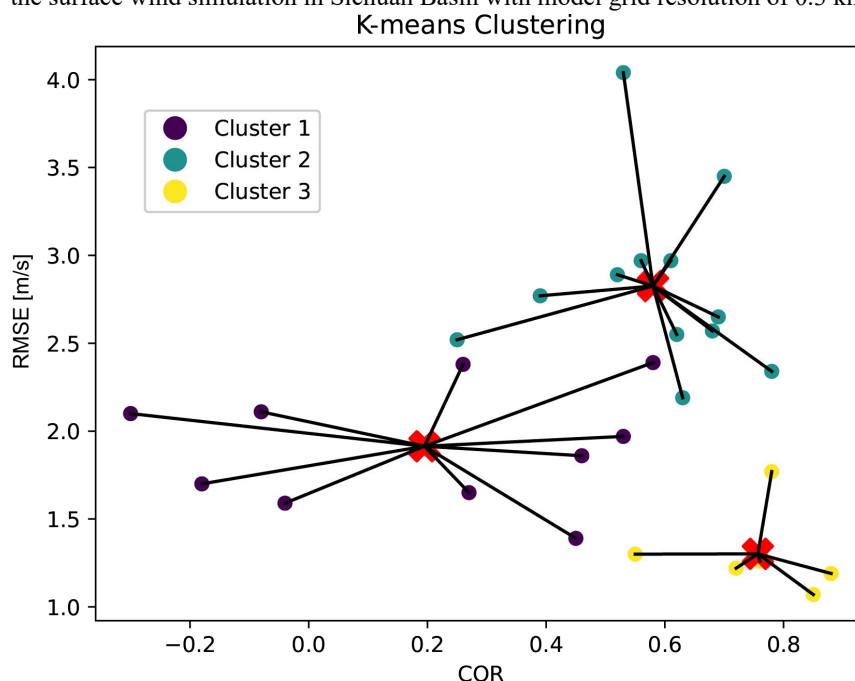
385 **3.4 K-means clustering analysis and performance in different types of events**

From the previous analysis, it is known that as the horizontal grid spacing of
 0.33 km is within the PBL gray zone resolution, QNSE scheme can better capture the
 trend of surface wind events over Sichuan Basin, while the bias produced by MYJ
 scheme is the minimum. The results also show the difference in different wind speed
 390 segment and different time in this region, but it is not significant. At the same time,
 Previous studies have indicated that the simulation of meteorological elements within
 the boundary layer is influenced by meteorological conditions such as circulation
 patterns. Therefore, it is necessary to further classify and analyze these 28 cases to
 understand the specific performance of PBL schemes in simulating surface wind
 395 events in Sichuan basin.

The K-means cluster method is used to divide the simulation results of 28
 surface wind events into three categories, as presented in Fig. 8. The RMSE of the
 cluster center of the first class is 1.9 m s^{-1} , and the COR is 0.2. A total of 10 events
 belong to this class, presenting the class with good RMSE but poor COR. At the
 400 cluster center of the second class, the RMSE is 2.85 m s^{-1} , and the COR is 0.6. A total
 of 12 events belong to this class, characterized by good COR but large bias. At last,
 the left 6 events belong to the third category, in which both RMSE and COR are very
 good for simulation, and the cluster center has the RMSE of 1.25 m s^{-1} , and COR of

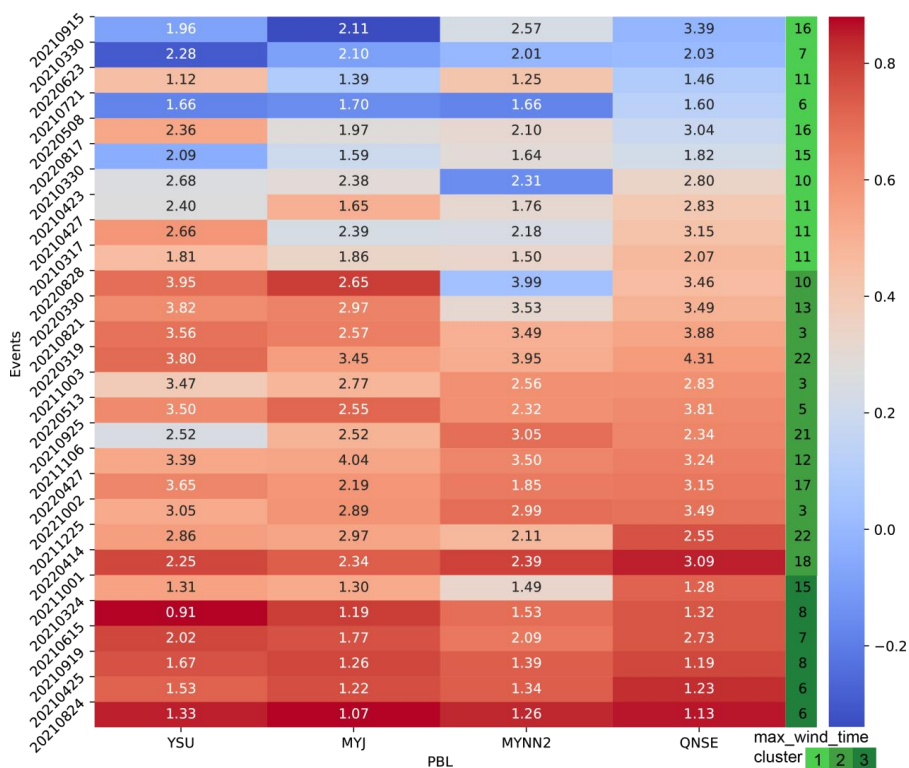


0.76. Furthermore, it is shown that among the three types of events, the QNSE
 405 scheme has the best simulation correlation coefficient, while the MYJ scheme has the
 smallest wind speed simulation error. This is consistent with the unclassified results,
 indicating that QNSE and MYJ schemes are relatively stable and reliable choices for
 the surface wind simulation in Sichuan Basin with model grid resolution of 0.3 km .



410 **Figure 8.** Scatter plot of K-means cluster analysis, the red cross symbol represents the
 cluster center.

According to the K-means analysis, it is found that different PBL schemes are
 very sensitive to the diurnal variation and circulation background of surface wind in
 the simulation of surface wind speed in the Basin, though there is no obvious seasonal
 415 difference. Figure 9 shows the RMSE and COR heat-maps of three types of events
 after cluster analysis, and peak time of gale is specially marked. It can be seen that the
 four PBL schemes have the least sensitivity to the event of class III. This kind of
 event is characterized by that the gale period basically occurs between 06:00 and
 08:00 UTC, which is also the period with the highest surface temperature and the
 most unstable atmospheric stratification in the region. What's more, in the events of
 420 class III, except for one thunderstorm gale event, the rest are all typical strong cold air
 induced surface wind processes, which indicates that the four PBL schemes have the
 good performance in simulating the typical strong cold air wind event occurred in the
 afternoon. As shown in Figure 10, the RMSE ranges from 0.21 m s^{-1} to 0.96 m s^{-1} , and
 425 the COR ranges from 0.05 to 0.19, with only one case having a difference of 0.3,
 which means that there is little difference between four PBL schemes.



430 **Figure 9.** Heat-map about the RMSE (numbers) and COR (coloring) of four PBL schemes for 28 near-surface wind simulations according to the cluster analysis. The information in the right column is gale moment (numbers) and classification label (coloring).

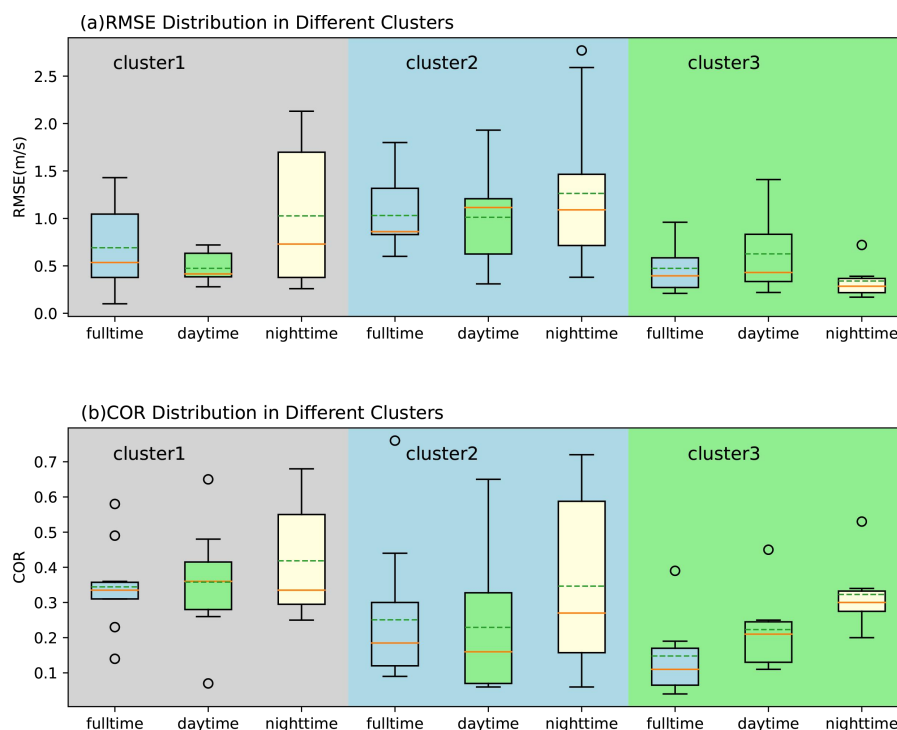


Figure 10. Box plots of the maximum differences during four PBL schemes in three types of events, with the green dotted line as the mean, the orange solid line as the median, and the circle as the outlier.

435

The most obvious differences among the four PBL schemes are mainly in the events of class I and II. Except for one southerly gale event belonging to class III, the other southerly wind events are classified into class I, indicating that the four PBL schemes often have good RMSE and poor COR for southerly wind events caused by convection in Sichuan Basin. In Figure 9, it is shown that in class I, the maximum wind speed often occurred in the two periods of 10:00 - 11:00 UTC and 15:00 - 16:00 UTC, and only two cases occurred at 06:00 - 07:00 UTC. The period of 10:00 - 16:00 UTC is the period when the atmospheric stratification in the basin changes from unstable to stable, and it is also the period when the inversion layer is established. In this kind of events, the difference between the maximum and minimum RMSE and COR obtained by different PBL schemes is as large as 1.43 m s⁻¹ and 0.58.

440

445

The simulation events of class II show the most significant differences among the four PBL schemes, and the characteristics such as gale occurrence time are significantly different from those in class I and class III. It is observed that the four PBL schemes often exhibit high CORR and high RMSE for surface wind events occurring in the early morning (17:00-22:00 UTC) and early afternoon (03:00-05:00 UTC), and these surface wind events are concentrated in dry and cold air scenarios. In this type the maximum difference between different PBL schemes can reach 1.49 m

450



455 s^{-1} and 0.76. In addition, Fig. 10 shows that the differences between different PBL
schemes in class I and class II events in the daytime are relatively small, while there
are greater differences at night. Meanwhile, in class III, the RMSE performance at
night is better than that in the daytime, but the COR is worse than that in the daytime.
460 Therefore, it can be concluded that there are obvious and diversified differences
among the simulation results shown by various PBL schemes under different types of
surface wind events.

4 Summary and conclusions

In this study, a horizontal resolution of 0.33 km which is within the PBL gray
zone resolution is employed to investigate the performance of four commonly used
465 PBL schemes on near-surface wind simulation over the Sichuan Basin. In China, the
near-surface wind prediction over Sichuan Basin has always a low score, and the
main focus of wind simulation is about the pollutant diffusion under stable weather
conditions at a horizontal resolution equals or greater than 1 km. Thus, we chose the
site of Guanghan Airport as the representation, and conducted a total of 112 WRF
470 sensitivity experiments, specifically focusing on 28 events with near-surface winds
exceeding $6 m s^{-1}$ by varying the PBL scheme, and assessed the impact of different
PBL schemes on wind speed and direction simulations. Subsequent analyses
considered factors such as diurnal variation of surface wind processes and circulation
background to gain further understanding of their influence on model sensitivity.
475 Therefore, the findings of our study offer the valuable insights in this region.

From our evaluation and analysis, the sensitivity of surface wind direction over
Sichuan Basin to the four commonly used PBL schemes is very low, and the
performance of MYNN2 is the worst when simulating the surface wind direction,
while the other three schemes are generally consistent with the observations, and the
480 MYJ scheme is the best for simulating NNE and NE winds. Our findings on wind
direction is agree with the finding in many other researches (Gómez-Navarro et al.,
2015; Tan et al., 2017; Shen and Du, 2023).

Generally speaking, no scheme can simulate the trend and wind speed of surface
wind events well at the same time, which is also mentioned by Cohen et al. (2015).
485 However, the 1.5-order QNSE local closure approximation scheme appears to be the
best for the temporal variation, while MYJ is the scheme with smallest simulation
error on wind speed. As the metrics RMSE and ME shows the similar characteristics,
K-means cluster analysis is employed based on the COR and RMSE, and the
simulation results are divided into three categories. The first category of events
490 showed poor correlation but small RMSE; the second category of events showed high
correlation but large RMSE; the third category of events showed high correlation
coefficient and small RMSE. Further analysis found that the four PBL schemes can
simulate the ground wind events caused by the typical strong cold air (occurring at
6:00-8:00 UTC), and there is little difference between them. For the surface wind
495 events occurring in the midnight to early morning, they are mainly concentrated in the
second category; while the evening to night and the southerly wind process are



mainly concentrated in the first category. Therefore, multi-cases studies and K-means clustering analysis gives us the hint that the simulation performance of the PBL schemes mainly depends on the prevailing weather conditions of each case, such as circulation backgrounds and the time of surface wind events.

Code and data availability. The Weather Research and Forecasting (WRF) model version 4.3.1 used in this study is freely available online and can be downloaded from https://www2.mmm.ucar.edu/wrf/users/download/get_source.html (Skamarock et al., 2008). The ERA5 data are available from ECMWF (<https://www.ecmwf.int/en/forecasts/datasets/reanalysis-datasets/era5>, last access: 23 June 2023, DOI: <https://doi.org/10.24381/cds.bd0915c6>, Hersbach et al., 2018). The observations and model output upon which this work is based are available from Zenodo (<https://doi.org/10.5281/zenodo.11328605>, Wang et al., 2024), and the data can also be obtained from pwd@cafuc.end.cn.

Author contributions. QW conceptualized the study and conducted the simulations. BZ, YY and GC analyzed the model results, and QW and BZ contributed to the interpretations. The original draft of the paper was written by QW, and all the authors took part in the edition and revision of it.

Competing interests. The contact author has declared that none of the authors has any competing interests.

Disclaimer. Publisher's note: Copernicus Publications remains neutral with regard to jurisdictional claims in published maps and institutional affiliations.

Acknowledgments. The authors acknowledge NCAR for the WRF model and ECMWF for the ERA5 reanalysis datasets.

Financial support. This research has been supported by the National Key Research and Development Program of China (grant no. 2022YFC3003902 and 2023YFC3007502), the National Natural Science Foundation of China (grant no. 42030611), and Sichuan Science and Technology Program (grant no. 2022NFSC0021 and 2023NSFSC0904).

References

Cohen, A. E., Cavallo, S. M., Coniglio, M. C., and Brooks, H. E.: A Review of Planetary Boundary Layer Parameterization Schemes and Their Sensitivity in Simulating Southeastern U.S. Cold Season Severe Weather Environments, *Wea. Forecasting*, 30, 591–612, <https://doi.org/10.1175/WAF-D-14-00105.1>, 2015.



- Cui, C. -X., Bao, Y. -X., Yuan, C. -S., Zhou, L. -Y., Jiao, S. -M, and Zong, C.: Influence of Different Boundary Layer Parameterization Schemes on the Simulation of an Advection Fog Process in Jiangsu, *Chinese J. Atmos. Sci.*, 42, 1344-1362, doi:10.3878/j.issn.1006-9895.1801.17212, 2018(in Chinese).
- 540 Chen, L., Li, G., Zhang, F., and Wang, C.: Simulation uncertainty of Near-Surface wind caused by boundary layer parameterization over the complex terrain, *Front. Energy Res.*, 8, <https://doi.org/10.3389/fenrg.2020.554544>, 2020.
- Coccia, M.: The effects of atmospheric stability with low wind speed and of air pollution on the accelerated transmission dynamics of COVID-19, *Int. J. Environ. Stud.*, 78, 1–27, <https://doi.org/10.1080/00207233.2020.1802937>, 2020.
- 545 Dudhia, J.: A history of mesoscale model development, *Asia-Pac. J. Atmos. Sci.*, 50, 121–131, <https://doi.org/10.1007/s13143-014-0031-8>, 2014.
- Feng, X., Zhang, Z., Guo, J. -P., and Wang, S. -G.: Multilayer inversion formation and evolution during persistent heavy air pollution events in the Sichuan Basin, China, *Atmos. Res.*, 286, 106691, doi: 10.1016/j.atmosres.2023.106691, 2023.
- 550 Gómez-Navarro, J. J., Raible, C. C., and Dierer, S.: Sensitivity of the WRF model to PBL parametrisations and nesting techniques: evaluation of wind storms over complex terrain, *Geosci. Model Dev.*, 8, 3349 – 3363, <https://doi.org/10.5194/gmd-8-3349-2015>, 2015.
- 555 Gao, D. -M., Li, Y. -Q., Jiang, X. -W., Li, J., and Wu, Y.: Influence of Planetary Boundary Layer Parameterization Schemes on the Prediction of Rainfall with Different Magnitudes in the Sichuan Basin Using the WRF Model, *Chinese J. Atmos. Sci.*, 40, 371-389, doi: 10.3878/j.issn.1006-9895.1503.14323, 2016.
- Hong, S., Noh, Y., and Dudhia, J.: A New Vertical Diffusion Package with an Explicit Treatment of Entrainment Processes, *Mon. Weather Rev.*, 134, 2318–2341, <https://doi.org/10.1175/mwr3199.1>, 2006.
- 560 Honnert, R., Couvreux, F., Masson, V., and Lancz, D.: Sampling the structure of convective turbulence and implications for Grey-Zone parametrizations. *Bound.-Layer Meteor.*, 160, 133–156, <https://doi.org/10.1007/s10546-016-0130-4>, 2016.
- 565 Hersbach, H., Bell, B., Berrisford, P., Biavati, G., Horányi, A., Muñoz Sabater, J., Nicolas, J., Peubey, C., Radu, R., Rozum, I., Schepers, D., Simmons, A., Soci, C., Dee, D., and Thépaut, J.- N.: ERA5 hourly data on pressure levels from 1959 to present, Copernicus Climate Change Service (C3S) Climate Data Store (CDS) [data set], <https://doi.org/10.24381/cds.bd0915c6>, 2018.
- 570 Janjić Z.: The step-mountain coordinate:Physical package, *Mon. Weather Rev.*, 118, 1429-1443, [https://doi.org/10.1175/1520-0493\(1990\)118<1429:TSMCPP>2.0.CO;2](https://doi.org/10.1175/1520-0493(1990)118<1429:TSMCPP>2.0.CO;2), 1990.
- Kibona, T. E.: Application of WRF mesoscale model for prediction of wind energy resources in Tanzania, *Sci. Afr.*, 7, e00302, <https://doi.org/10.1016/j.sciaf.2020.e00302>, 2020.
- 575 Li, Y. -P., Wang, D. -H., and Yin, J. -F.: Evaluations of different boundary layer schemes on low-level wind prediction in western Inner Mongolia, *Acta*



- Scientiarum Naturalium University Sunyatseni, 57(4), 16-29, doi: 10.13471/
580 j.cnki. acta. snus. 2018.04.003, 2018(in Chinese).
- Liu, M. -J., Zhang, X., and Chen, B. -D.: Assessment of the suitability of planetary
boundary layer schemes at “grey zone” resolutions, *Chinese J. Atmos. Sci.*, 42
(1), 52-69, doi: 10.3878/ j.issn. 1006- 9895. 1704.16269, 2018.
- Liu, F., Sun, F., Liu, W., Wang, T., Hong, W., Wang, X., and Lim, W. H.: On wind
585 speed pattern and energy potential in China, *Appl. Energy*, 236, 867–876,
<https://doi.org/10.1016/j.apenergy.2018.12.056>, 2019.
- Leung, A. C. W., Gough, W. A., Butler, K., Mohsin, T., and Hewer, M. J.:
Characterizing observed surface wind speed in the Hudson Bay and Labrador
regions of Canada from an aviation perspective, *Int. J. Biometeorol.*, 66,
590 411–425, <https://doi.org/10.1007/s00484-020-02021-9>, 2020.
- Liu, Y., Zhou, Y., and Lu, J.: Exploring the relationship between air pollution and
meteorological conditions in China under environmental governance, *Sci. Rep.*,
10, <https://doi.org/10.1038/s41598-020-71338-7>, 2020.
- Li, X., Hussain, S. A., Sobri, S., and Said, M. S. M.: Overviewing the air quality
595 models on air pollution in Sichuan Basin, China, *Chemosphere*, 271, 129502,
<https://doi.org/10.1016/j.chemosphere.2020.129502>, 2021.
- Manasseh, R., and Middleton, J. H.: The surface wind gust regime and aircraft
operations at Sydney Airport, *J. Wind Eng. Ind. Aerodyn.*, 79, 269–288,
[https://doi.org/10.1016/s0167-6105\(97\)00293-6](https://doi.org/10.1016/s0167-6105(97)00293-6), 1999.
- 600 Ma, Y. -Y., Yang, Y., Hu, X. M., Qi, Y. -C., and Zhang, M.: Evaluation of Three
Planetary Boundary Layer Parameterization Schemes in WRF Model for the
February 28th, 2007 Gust Episode in XinjianG, *Desert and Oasis Meteorology*,
8(3), 8-18, doi: 10. 3969/ j. issn. 1002-0799. 2014.03.002, 2014 (in Chinese).
- Mu, Q. -C., Wang, Y. -W., Shao, K., Wang, L. -F., and Gao, Y. Q.: Three planetary
605 boundary layer parameterization schemes for the preliminary evaluation of near
surface wind simulation accuracy over complex terrain, *Res. Sci.*, 39, 1319- 1360,
doi: 10.18402/resci.2017.07.12, 2017.
- Mi, L., Shen, L., Yan, H., Cai, C., Zhou, P., and Li, K.: Wind field simulation using
WRF model in complex terrain: A sensitivity study with orthogonal design,
610 *Energy*, 285, 129411, <https://doi.org/10.1016/j.energy.2023.129411>, 2023.
- Nakanishi, M., and Niino, H.: Development of an improved turbulence closure model
for the atmospheric boundary layer, *J. Meteorol. Soc. Jpn.*, 87, 895–912,
<https://doi.org/10.2151/jmsj.87.895>, 2009.
- Prieto-Herráez, D., Frías-Paredes, L., Cascón, J. M., Lagüela-López, S., Gastón, M.,
615 Sevilla, M. I. A., Martín-Nieto, I., Fernandes-Correia, P., Laiz-Alonso, P.,
Carrasco-Díaz, O., Blázquez, C. S., Hernández, E., Ferragut-Canals, L., and
González-Aguilera, D.: Local wind speed forecasting based on WRF-HDWind
coupling, *Atmos. Res.*, 248, 105219,
<https://doi.org/10.1016/j.atmosres.2020.105219>, 2020.
- 620 Pan, L., Liu, Y., Roux, G., Cheng, W., Liu, Y., Ju, H., Jin, S., Feng, S., Du, J., and
Peng, L.: Seasonal variation of the surface wind forecast performance of the



- high-resolution WRF-RTFDDA system over China, *Atmos. Res.*, 259, 105673, <https://doi.org/10.1016/j.atmosres.2021.105673>, 2021.
- 625 Qi, X., Ye, Y., Xiong, X., Zhang, F., and Shen, Z.: Research on the adaptability of SRTM3 DEM data in wind speed simulation of wind farm in complex terrain, *Arab. J. Geosci.*, 14, <https://doi.org/10.1007/s12517-020-06326-2>, 2021.
- Sukoriansky, S., Galperin, B., and Perov, V.: A quasi-normal scale elimination model of turbulence and its application to stably stratified flows, *Nonlinear Process Geophys.*, 13, 9–22, <https://doi.org/10.5194/npg-13-9-2006>, 2006.
- 630 Skamarock, W. C., Klemp, J. B., Dudhia, J., Gill, D. O., Barker, D., Duda, M. G., Huang, X. Y., Wang W., and Powers, J. G.: A description of the Advanced Research WRF version 3, NCAR Technical note-475+ STR, <https://doi.org/10.5065/D68S4MVH>, 2008 (data available at https://www2.mmm.ucar.edu/wrf/users/download/get_source.html, last access: 635 28 October 2021).
- Shin, H. -H., and Hong, S.: Representation of the Subgrid-Scale turbulent transport in convective boundary layers at Gray-Zone resolutions, *Mon. Weather Rev.*, 143, 250–271, <https://doi.org/10.1175/mwr-d-14-00116.1>, 2015.
- 640 Salfate, I., MariN, J., Cuevas, O., and Montecinos, S.: Improving wind speed forecasts from the Weather Research and Forecasting model at a wind farm in the semiarid Coquimbo region in central Chile, *Wind Energy*, 23, 1939–1954, <https://doi.org/10.1002/we.2527>, 2020.
- Shi, H., Dong, Z., Xiao, N., and Huang, Q.: Wind Speed Distributions Used in Wind Energy Assessment: A Review, *Front. Energy Res.*, 9: 769920, doi: 645 10.3389/fenrg.2021.769920, 2021.
- Shen, Y., and Du, Y.: Sensitivity of boundary layer parameterization schemes in a marine boundary layer jet and associated precipitation during a coastal warm-sector heavy rainfall event, *Front. Earth Sci.* 10,1085136, doi: 10.3389/feart.2022.1085136, 2023.
- 650 Tan, J., Zhang, Y., Ma, W., Yu, Q., Wang, Q., Fu, Q., Zhou, B., Chen, J., and Chen, L.: Evaluation and potential improvements of WRF/CMAQ in simulating multi-levels air pollution in megacity Shanghai, China, *Stoch. Environ. Res. Risk Assess.*, 31, 2513–2526, <https://doi.org/10.1007/s00477-016-1342-3>, 2017.
- 655 Tiesi, A., Pucillo, A., Bonaldo, D., Ricchi, A., Carniel, S., and Miglietta, M. M.: Initialization of WRF model simulations with sentinel-1 wind speed for severe weather events, *Front. Mar. Sci.*, 8, <https://doi.org/10.3389/fmars.2021.573489>, 2021.
- Wang, Y., Zhang, L., Hu, J., and Zhang, Y.: Verification of WRF Simulation Capacity on PBL Characteristic and Analysis of Surface Meteorological Characteristic over Complex Terrain, *Plateau Meteorol.*, 29(6), 1397-1407, doi:CNKI:SUN:GYQX.0.2010-06-005, 2010(in Chinese).
- 660 Wang, C. -G., Shen, Y. -J., Luo, F., Cao, L., Yan, J. -D., and Jiang, H. -M.: Comparison and analysis of several planetary boundary layer schemes in WRF model between clear and overcast days, *Chinese J. Geophys.*, 60, 141-153, doi:



- 665 10.6038/cjg20170307, 2017.
- Wu, A. -N., Li, G. -P., Shi, C. -Y., and Qin, L. -L.: Numerical Simulation Analysis of a Gale Weather in the Dam Area of Baihetan Hydropower Station by Using the Subgrid-scale Terrain Parameterization Scheme, *Plateau and Mountain Meteorol. Res.*, 42, 222-230, doi: 10.3969/j.issn.1674-2184.2022.03.003, 2022 (in Chinese).
- 670 Wang, Q., Zeng, B., Chen, G., and Li, Y.: Simulation performance of different planetary boundary layer schemes in WRF V4.3.1 on wind field over Sichuan Basin within “Gray zone” resolution, Zenodo [data set], <https://doi.org/10.5281/zenodo.11328605>, 2024.
- 675 Xu, W., Ning, L., and Luo, Y.: Applying satellite data assimilation to wind simulation of coastal wind farms in Guangdong, China, *Remote Sens.*, 12, 973, <https://doi.org/10.3390/rs12060973>, 2020.
- Xiang, T., Zhi, X., Guo, W., Lyu, Y., Ji, Y., Zhu, Y., Yin, Y., and Huang, J.: Ten-Meter wind speed forecast correction in southwest China based on U-Net neural network. *Atmosphere*, 14, 1355, <https://doi.org/10.3390/atmos14091355>, 2023.
- 680 Yang, G. -Y., Wu, X., and Zhou, H.: Effect analysis of WRF on wind speed prediction at the coast wind power station of Fujian province, *J. Meteorol. Sci.*, 34(5), 530-535, doi:10.3969/2013JMS.0014, 2014(in Chinese).
- 685 Yu, S., Tao, N., He, J. -J., Ma, Z. -F., Liu, P., Xiao D. -X., Hu, J. -F., Yang J. -C., and Yan, X. L.: Classification of circulation patterns during the formation and dissipation of continuous pollution weather over the Sichuan Basin, China, *Atmos. Environ.*, 223, 1-18, doi: 10.1016/j.atmosenv.2019.117244, 2020.
- Yang, J., and Shao, M.: Impacts of Extreme air pollution Meteorology on air quality in China, *J. Geophys. Res.-Atmos.*, 126, <https://doi.org/10.1029/2020jd033210>, 2021.
- 690 Yan, H., Mi, L., Shen, L., Cai, C., Liu, Y., & Li, K.: A short-term wind speed interval prediction method based on WRF simulation and multivariate line regression for deep learning algorithms, *Energy Conv. Manag.*, 258, 115540, <https://doi.org/10.1016/j.enconman.2022.115540>, 2022.
- 695 Yu, E. -T., Bai, R., Chen, X., and Shao, L.: Impact of physical parameterizations on wind simulation with WRF V3.9.1.1 under stable conditions at planetary boundary layer gray-zone resolution: a case study over the coastal regions of North China, *Geosci. Model Dev.*, 15, 8111–8134, <https://doi.org/10.5194/gmd-15-8111-2022>, 2022.
- 700 Zhang, B. -H., Liu, S. -H., and Ma, Y. -J.: The effect of MYJ and YSU schemes on the simulation of boundary layer meteorological factors of WRF, *Chinese J. Geophys.*, 55, 2239-2248, doi: 10.6038/j.issn.0001-5733.2012.07.010, 2012.
- Zhang, X. -P., and Yin, Y.: Evaluation of the four PBL schemes in WRF Model over complex topographic areas, *Trans. Atmos. Sci.*, 36(1), 68-76, doi:10.13878/j.cnki.dqkxxb.2013.01.008, 2013(in Chinese).
- 705 Zhang, L., Xin, J., Yin, Y., Chang, W., Xue, M., Jia, D., and Ma, Y.: Understanding the major impact of planetary boundary layer schemes on simulation of vertical wind

<https://doi.org/10.5194/egusphere-2024-1532>

Preprint. Discussion started: 24 June 2024

© Author(s) 2024. CC BY 4.0 License.



structure, *Atmosphere*, 12, 777, <https://doi.org/10.3390/atmos12060777>, 2021.